



## High-Gain Cubic Boost Converter Analysis with Hybrid ANN-Incremental Conductance MPPT for Solar PV Systems

Ali M. Jasim<sup>1\*</sup>, Alaa Hussein Abdulaal<sup>2</sup>, Baraa M. Albaker<sup>2</sup>, Muwafaq Shyaa Alwan<sup>1</sup>

<sup>1</sup> Department of Network Engineering, College of Engineering, Al-Iraqia University, Baghdad 10054, Iraq

<sup>2</sup> Department of Electrical Engineering, College of Engineering, Al-Iraqia University, Baghdad 10054, Iraq

Corresponding Author Email: [drali7819@gmail.com](mailto:drali7819@gmail.com)

Copyright: ©2024 The authors. This article is published by IETA and is licensed under the CC BY 4.0 license (<http://creativecommons.org/licenses/by/4.0/>).

<https://doi.org/10.18280/mmep.111216>

### ABSTRACT

**Received:** 6 August 2024

**Revised:** 13 October 2024

**Accepted:** 20 October 2024

**Available online:** 31 December 2024

#### Keywords:

*solar photovoltaic panel, power electronic converters, high-gain cubic boost converter, maximum power point tracking, artificial neural network, incremental conductance*

The demand for renewable energy in power systems is rapidly increasing, and various algorithms can efficiently and accurately track the maximum power point (MPP). This paper compares and analyses multiple control techniques for maximum power point tracking (MPPT) in photovoltaic systems under changing irradiance, temperature, and load characteristics, utilizing three algorithms: incremental conductance (INC), artificial neural network (ANN), and Hybrid INC-ANN. Three MPPT algorithms were developed for a standalone photovoltaic system with a high-gain cubic boost converter (HG-CBC) to optimize the solar panel's MPP. The performance of these controllers is evaluated using MATLAB/SIMULINK under varying irradiance and temperature conditions. The statement indicates that at 1000 W/m<sup>2</sup>, the power output efficiency of INC is lowest at 83.79%. In comparison, the hybrid ANN-INC efficiency and ANN algorithms registered at 97.48% and 88.94%, respectively. The simulation shows that the INC algorithm has the lowest performance regarding time response, while the Hybrid INC-ANN and ANN algorithms perform better than the INC.

## 1. INTRODUCTION

The rapid increase in the global population leads to a higher demand for energy. Traditional power generation methods, due to their emission of greenhouse gases, not only harm the environment but also contribute to energy shortages as they strive to meet this growing demand [1]. Recent research identifies advances and challenges in renewable energy across diverse regions. In USA, a 35-year study [2] investigated public attitudes on renewable power growth, revealing the rise of community acceptability.

Photovoltaic energy conversion systems have emerged as a key area in renewable energy, driven by significant advancements in photovoltaic (PV) cell technology, energy conversion efficiency, array size, power electronics, and control methods for optimal power point tracking [3]. Despite its growing popularity and environmental benefits, photovoltaic energy faces many challenges due to its dependence on environmental factors. Research opportunities in photovoltaic generating systems can help expand the reach of solar power globally. The MPPT function optimizes the electricity generated by solar panels by managing their optimal operating voltage and current [4]. This is achieved by continuously monitoring the solar panel array's voltage ( $V_{pv}$ ) and current ( $I_{pv}$ ) to adjust electricity extraction accordingly. MPPT is essential for optimizing energy use in PV systems. This power extraction control is crucial due to solar panels' non-linear Voltage/Current (V/I) curve, which changes with solar energy and panel temperature [5]. A PV module's output

depends on its environment, with a single MPP corresponding to specific solar irradiation and cell temperature. Therefore, operating a PV module at MPP is essential for maximizing energy production. Maximum power point tracking (MPPT) technologies have been developed to achieve this [6]. Numerous MPPT algorithms have been developed, varying in applicability, complexity, accuracy, sensor requirements, cost, popularity, and other factors [7]. The traditional methods include short-circuit current [8], open-circuit voltage [9], perturb and observe (P&O) [10], INC [11], and hill-climbing [12]. At the same time, soft computing-based techniques consist of fuzzy logic controllers [13], bat algorithms (BA) [14], particle swarm optimization [15], genetic algorithms (GA) [16], and more. The simplicity of the INC approach has intrigued scholars. However, it inevitably deviates from the MPP during rapid changes in solar irradiation, leading to steady-state oscillation issues [17]. ANN effectively handle non-linear PV module characteristics and environmental variability, making them quick at tracking the MPP [18]. An effective DC-DC converter with high voltage gain is necessary to run a solar photovoltaic system at the MPPT under rapidly changing air conditions [19]. The cubic boost converter (CBC) delivers high voltage gain, particularly at low duty ratios, making it suitable for solar photovoltaic applications. Besides its high voltage gain, the CBC topology also reduces voltage stress on switches, diodes, and capacitors, offering an additional advantage [20].

Environmental factors, like dust accumulation, irradiance, and temperature, have a realistic influence on the performance

of a PV module [21]. While these factors are important to consider in providing reliable data entry, this paper focuses on modeling the parameters of the PV module and provide a reliable control technique to extract maximum power from the module. It proposes a hybrid MPPT that integrates ANN with the INC technique, capitalizing on its dynamic response to sudden atmospheric changes. The ANN-based MPPT demonstrates robust tracking control and stability against internal system parameters and load uncertainties, as verified

using MATLAB/Simulink.

## 2. COMPLETE SYSTEM ARCHITECTURE

The system's layout configuration, as illustrated in Figure 1, consists of a PV panel, DC-DC converter CBC, INC MPPT algorithm, ANN algorithm, Hybrid INC-ANN MPPT algorithm, Pulse-Width Modulation (PWM) control, and load.

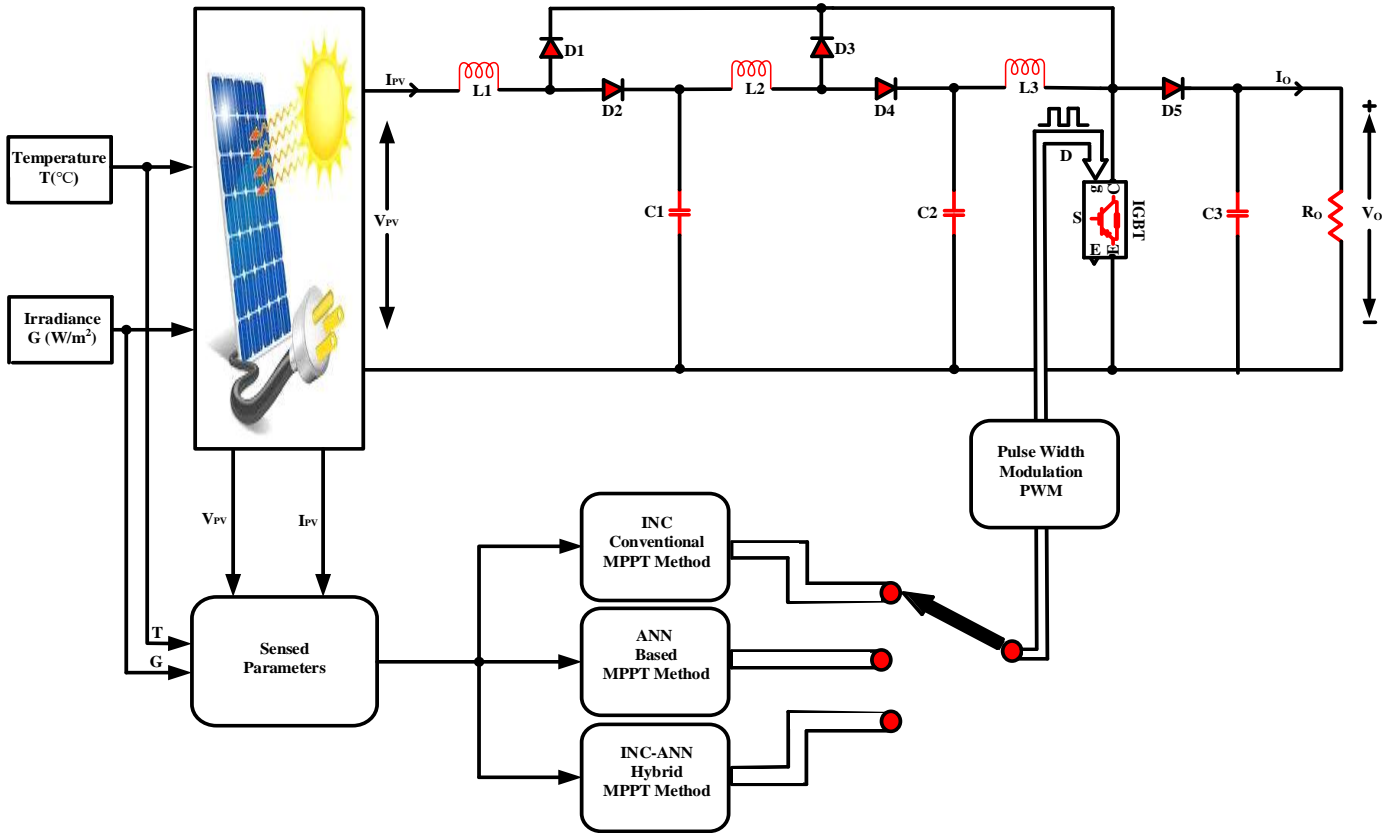


Figure 1. Solar PV system coupled to a load by MPPT

## 3. MODELING FIVE PARAMETERS MODEL

The concept of the PV model is to construct the PV module's current-voltage (I-V) curve. The classical photovoltaic model computes the complete photocurrent  $I_c$ , which is determined by Eq. (1) as illustrated in Figure 2 [22], incorporates a solitary diode linked in parallel with a light-generated current source  $I_{ph}$ , is determined by Eq. (2) accompanied by a series resistance is indicated as in ohms  $R_{se}$  and a parallel admittance,  $G_{pa}$  (where  $G_{pa} = 1/R_{pa}$ ). This particular model, referred to as the five-parameter model [23], encompasses  $I_{ph}$ ,  $I_s$ ,  $A$ ,  $R_{se}$ , and  $R_{pa}$ . Despite its benefits, its precision decreases under lower irradiance conditions, through the application of Kirchhoff's Current Law (KCL) [24].

$$I_c = n_p I_{ph} - n_p I_s \left[ \exp \left( \frac{V_o + I_c R_{se}}{n_s K_B T} \right) - 1 \right] - G_{pa} (V_o + I_c R_{se}) \quad (1)$$

Photovoltaic arrays are constructed by combining solar cells in series  $n_s$  and panels in parallel  $n_p$ . The idealist factor is represented by  $A$ . Boltzmann's constant,  $K_B$ , has a value of  $1.38 \times 10^{-23}$  J/K.  $T$  signifies the temperature of the p-n junction

in Kelvin (K). The electron charge is represented as  $q$  and holds a value of  $1.6 \times 10^{-19}$  in coulomb [C] [25]. Where  $STC$  stands for standard test conditions ( $1000 \text{ W/m}^2$  and  $25^\circ\text{C}$ ), and  $G_{ir}$  denotes the irradiance in watts per square meter ( $\text{W/m}^2$ ). The temperature corresponding to  $ref$ , is designated as  $T_{ref}$  and is set at  $25^\circ\text{C}$ . Figure 3 illustrates the internal photocurrent model block diagram.

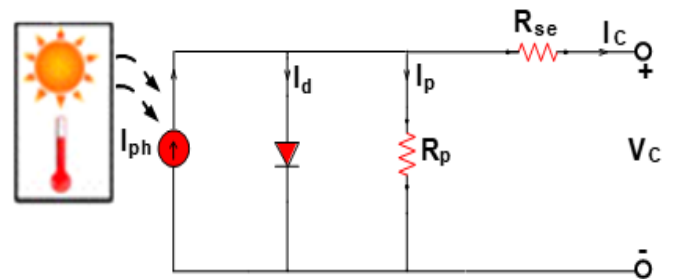


Figure 2. Complete diagram of the five parameters model

$$I_{ph} = \frac{G_{ir}}{G_{STC}} [I_{sc,STC} + K_{sc}(T - T_{ref})] \quad (2)$$

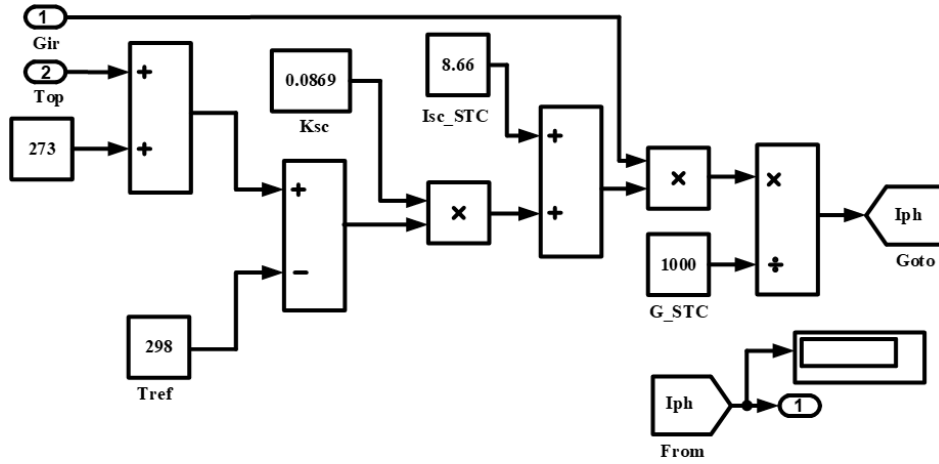


Figure 3. Equivalent circuit diagram of photocurrent model

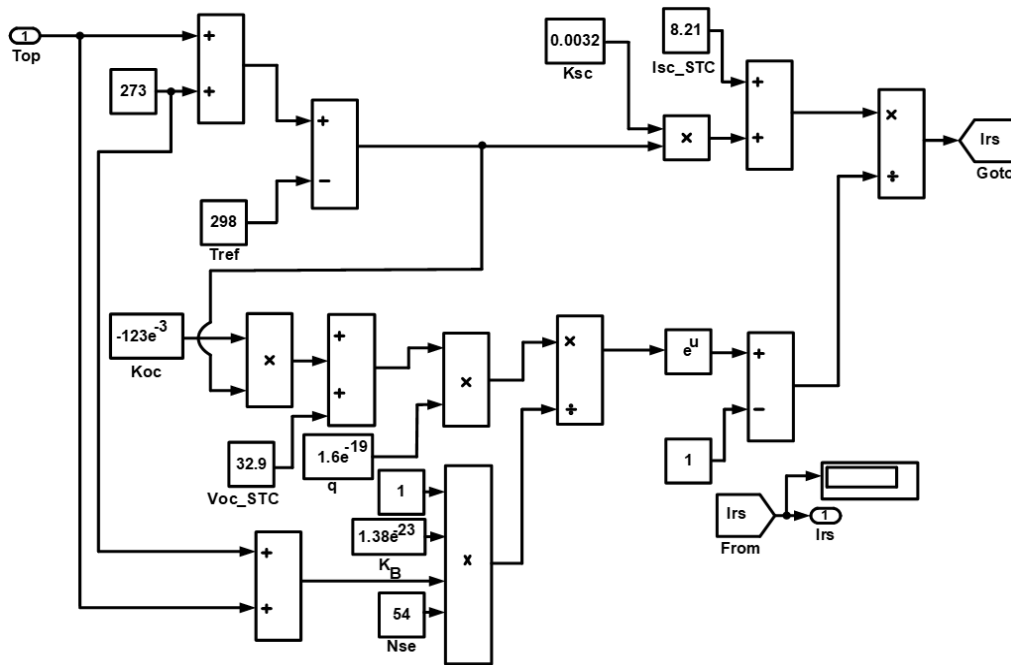


Figure 4. Equivalent circuit diagram of reverse saturation current model

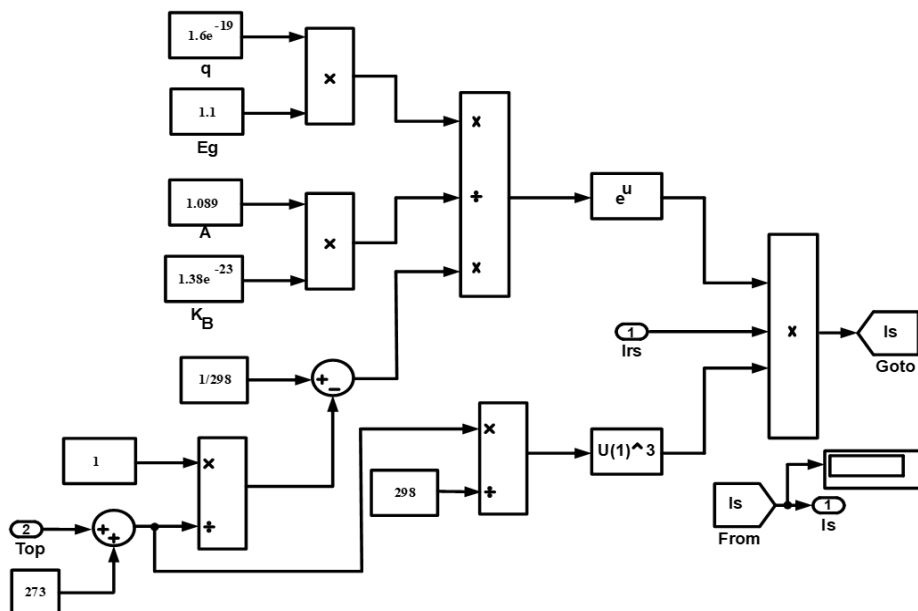


Figure 5. Equivalent circuit diagram of saturation current model

**Table 1.** Solar-powered CBC parameters

Parameters	Value
Parallel strings	1
Series-connected modules per string	1
Maximum power ( $P_{MP}$ )	250.2 W
Open circuit voltage ( $V_{oc}$ )	37.3 V
Short current ( $I_{sc}$ )	8.66 A
Voltage maximum power ( $V_{MP}$ )	30.7 V
Current maximum power ( $I_{MP}$ )	8.15 A
Photovoltaic current ( $I_{ph}$ )	8.706 A
Saturation current of the panel	4.1579e-10 A
Diode ideality factor	1.0189
Solar cells in series $n_s$	60
Solar cells in parallel $n_p$	1
Series resistance $R_{se}$	0.2373 $\Omega$
Parallel resistance $R_{pa}$	240.60 $\Omega$
Switching frequency	10 K
Inductor	$L_1=0.2e-3$ H
	$L_2=0.3e-3$ H
	$L_3=0.1e-3$ H
Capacitors	$C_1=6e-3$ F
	$C_2=3e-3$ F
	$C_3=2e-3$ F

Diode reverse saturation current ( $I_{rs}$ ) depends on the temperature coefficient, which includes ( $K_{sc}$ ) short is the cell's short-circuit current temperature coefficient (A/K), and ( $K_{ov}$ ), the cell's open-circuit voltage temperature coefficient (V/K) [26].  $K_{VT}$  thermal voltage coefficient = 26 mV at 300 K, which is determined using Eq. (3). Figure 4 represents the internal block diagram of diode reverse saturation current.

$$I_{rs} = \frac{I_{sc\_STC} + K_{sc}(T - T_{ref})}{\exp(V_{oc\_STC} + K_{ov}(T - T_{ref})/AK_{VT}) - 1} \quad (3)$$

The diode saturation current ( $I_s$ ) is influenced by temperature and the semiconductor material's band-gap energy

( $E_g$ ), as described in Eq. (4). Figure 5 illustrates the internal diagram of the diode saturation current model. The parameters for this solar PV module simulation are listed in Table 1. The simulated PV module is the 1Soltech 1STH-250-WH.

$$I_s = I_{rs} \cdot \left(\frac{T}{T_{ref}}\right)^3 \cdot \exp\left[\frac{qE_g}{AK_B} \left(\frac{1}{T_{ref}} - \frac{1}{T_{op}}\right)\right] \quad (4)$$

#### 4. CUBIC BOOST CONVERTER

A fundamental CBC [27], with high gain, as illustrated in Figure 6, is composed of a solitary semiconducting switch (S), a trio of inductors ( $L_1, L_2,$  and  $L_3$ ), three capacitors ( $C_1, C_2,$  and  $C_3$ ), five diodes ( $D_1, D_2, D_3, D_4,$  and  $D_5$ ), and a resistive load ( $R_o$ ). This high-gain cubic boost converter utilizes a single switch (S) to regulate the  $V_{out}$  and encompasses two distinct operational modes [27].

The operational configuration denoted as the first mode of the high-gain CBC is visually illustrated in Figure 7. In this scenario, the semiconducting switch (S) is activated. Simultaneously, two diodes ( $D_1$  and  $D_3$ ) are conducting, whereas the remaining three ( $D_2, D_4,$  and  $D_5$ ) remain open-circuited. The input source initiates the charging of the inductor ( $L_1$ ), while the inductor ( $L_2$ ) becomes energized through the voltage across the capacitor ( $C_1$ ). Lastly, the inductor ( $L_3$ ) is stimulated by the voltage across the capacitor ( $C_2$ ). The current for the resistive load (R) is supplied through the voltage of the capacitor ( $C_3$ ).

The second operational mode of the high-gain cubic boost converter. is depicted in the circuit diagram shown in Figure 8. In this configuration, the switch (S) is turned off. While diodes  $D_1$  and  $D_3$  function as open circuits, diodes  $D_2, D_4,$  and  $D_5$  are conducting. The inductors ( $L_1, L_2,$  and  $L_3$ ) will be disengaged, capacitors ( $C_1, C_2,$  and  $C_3$ ) are in a certain state.

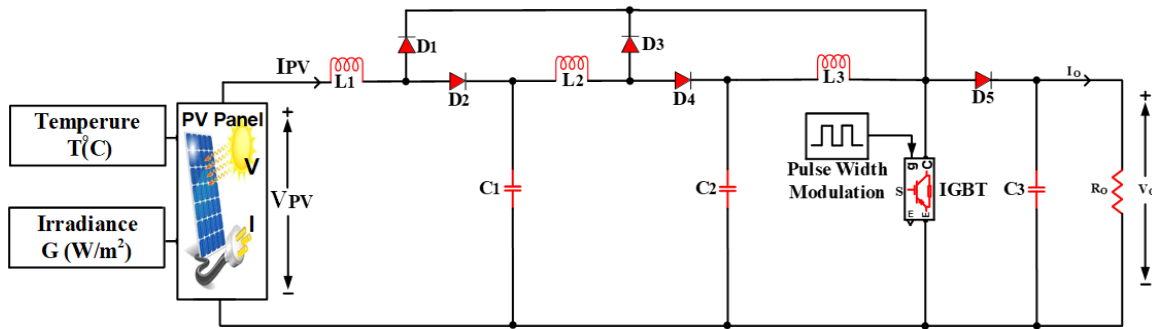


**Figure 6.** Cubic boost converter

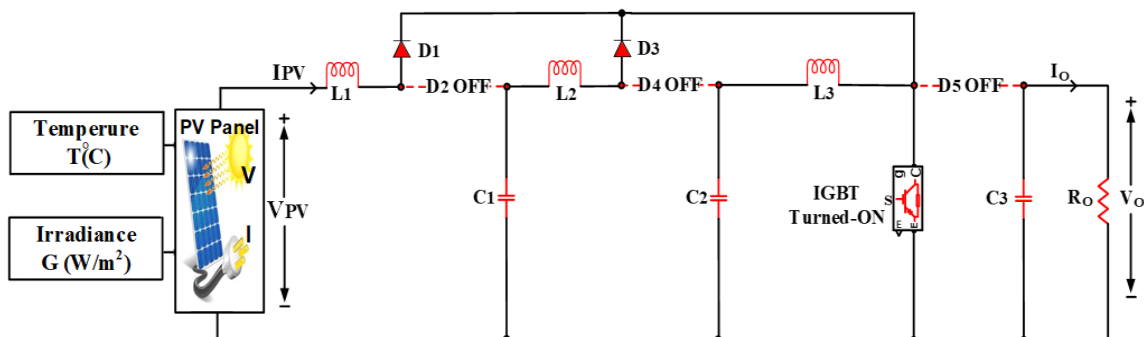


**Figure 7.** Cubic boost converter on state

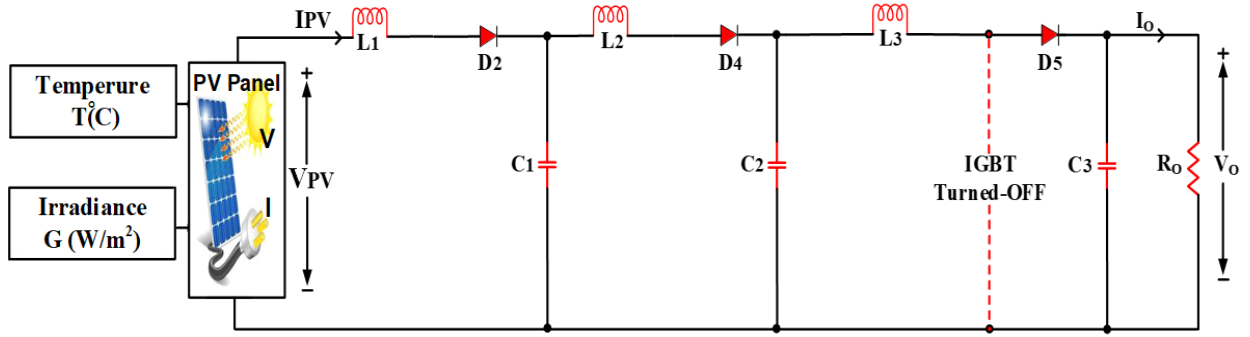


Figure 8. Cubic boost converter off state

Applying KVL determines the voltage across inductors ( $L_1$ ,  $L_2$ , and  $L_3$ ), as shown in Eq. (5) and Eq. (6).

$$V_{L1} = V_{PV}; V_{L2} = V_{C1}; V_{L3} = V_{C2} \quad (5)$$

$$V_{L1} = V_{PV} - V_{C1}; V_{L2} = V_{C1} - V_{C2}; V_{L3} = V_{C2} - V_O \quad (6)$$

The voltage across the capacitor  $V_{C1}$  is expressed as Eq. (7), where duty cycle, ( $d$ ):

$$V_{C1} = \frac{V_{PV}}{1 - D} \quad (7)$$

The voltage across the capacitor  $V_{C2}$  is expressed as Eq. (8):

$$V_{C2} = \frac{V_{PV}}{1 - D} \quad (8)$$

By substituting the value of  $V_{C1}$  in terms of the input voltage  $V_{PV}$ , we can express  $V_{C2}$  as shown in Eq. (9):

$$V_{C2} = \frac{V_{PV}}{(1 - D)^2} \quad (9)$$

The voltage across the resistance  $V_O$  is expressed as Eq. (10):

$$V_O = \frac{V_{C2}}{1 - D} \quad (10)$$

The average current passing through the output diode corresponds to the output current  $I_O$ ; hence Eq. (11):

$$I_O = I_{D5} = \frac{V_O}{R_O} \quad (11)$$

By substituting the value of  $V_{C2}$  in terms of the input voltage  $V_{PV}$ , the gain of the voltage ratio is calculated as Eq. (12):

$$\frac{V_O}{V_{PV}} = \frac{1}{(1 - D)^3} \quad (12)$$

## 5. MPPT

Efficient implementation of MPPT is crucial, given the formidable challenge of achieving maximum power extraction from solar photovoltaic systems [28]. The utilization of MPPT facilitates the alignment of solar PV and load impedances.

There are diverse approaches to modulating the duty cycle of the DC-DC converter to extract the  $P_{max}$ . Ideally, photovoltaic systems should continuously operate at their MPP under all operating conditions, which include all possible combinations of ambient temperature and solar irradiance levels. A solar photovoltaic system's voltage, current, and power output characteristics vary depending on solar irradiance levels and temperature conditions for a particular load. An MPPT system does just that: it constantly observes the MPP. By utilizing an algorithm, the converter is fine-tuned whenever its conditions change, thus maintaining a panel's output power at its maximum for a given period. Essentially, the tracking system usually measures the current and voltage to determine how much power the PV panel can provide. The algorithm then uses that information to calculate how much the circuit needs to be adjusted to produce more power from the panel. These changes to the converter come in the form of adjustments in something called the duty cycle, which controls the converter. Consequently, this leads to an alteration in the  $V_{out}$ , with the  $V_{in}$  remaining consistent. Within a converter linked to a PV panel, this increase in output voltage originates from the converter, allowing a higher input current to pass through it. Elevating the converter's duty cycle simultaneously amplifies the current streaming from the PV panel to the converter. As a result, the PV panel transitions from its current operating point on the I-V curve to a subsequent point characterized by an increased current output, which is a leftward shift. This transition results in a decrease in the voltage output of the PV panel. Once the panel's operating point becomes adjustable, an algorithm can be employed to control this shift, thereby forming an MPPT system. While various algorithms may manifest distinct behaviors, this fundamental concept serves as the basis for most MPPT systems [29]. Given the unique attributes and constraints of different algorithms, this study utilizes the hybrid maximum power point tracking, which contains two methods: INC and ANN.

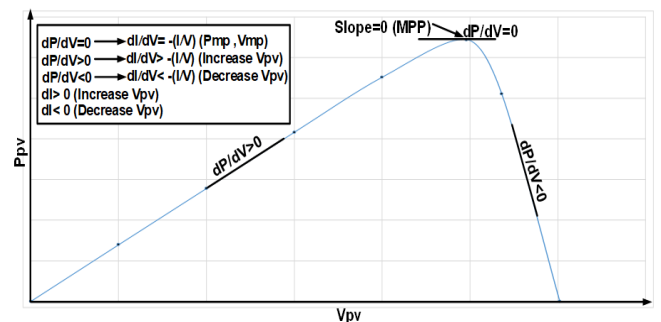


Figure 9. INC method schematic diagram

$$\frac{dp}{dV} < 0 = \frac{dI}{dV} < -\frac{I}{V} \quad (15)$$

## 5.2 ANN

ANN plays a significant part in enhancing the performance of MPPT for PV systems. This role becomes outstanding in complex and dynamic environments where traditional methods may fail to perform well. On the other hand, ANNs function primarily to learn and adapt to the nonlinear characteristics of PV systems so that the MPP can be efficiently tracked [31].

However, INC's efficiency can be reduced by fast-changing irradiance and partial shading conditions. ANNs make a considerable improvement in this area. An ANN can learn complicated nonlinear relationships between these input parameters, irradiance, temperature, and the MPP to make an ANN-based MPP predictor.

The typical ANN model will have numerous layers of neurons, where every layer performs a weighted sum of its inputs and is then fed through a non-linear activation function like a sigmoid function, as shown in Eq. (16):

$$y = f\left(\sum_i W_i X_i + b\right) \quad (16)$$

where,  $y$  is the output,  $X_i$  are the inputs,  $W_i$  are the weights,  $b$  is the bias, and  $f$  is the activation function. During training, the ANN adjusts its weights  $W_i$  and biases  $b$  to minimize the error between its predicted output and the actual MPP, using techniques like backpropagation and gradient descent. The loss function  $L$  used for this optimization is often the mean squared error (MSE), as shown in Eq. (17).

$$L = \frac{1}{n} \sum_{i=1}^n (P_{pred,i} - P_{actual,i})^2 \quad (17)$$

where,  $P_{pred,i}$  is the power predicted by the ANN and  $P_{actual,i}$  is the actual measured power.

The ANN [32] is structured as a feedforward neural network. It consists of an input layer that receives voltage ( $V_{pv}$ ) and current ( $I_{pv}$ ) inputs, hidden layers configured with a specified number of neurons to capture non-linear relationships, and an output layer that generates the predicted duty cycle ( $D$ ) for PWM control.

The training process begins with data collection under various irradiance and temperature conditions as input and the values of  $V_{MP}$  as output to ensure diverse scenarios. To achieve convergence, the network is trained using backpropagation with a learning rate of 0.01 over 1100 epochs. A 5-fold cross-validation method is employed to evaluate performance robustly with an 80-20 train-test split.

Parameter selection is crucial for the network's efficiency. The sigmoid activation function is used in the hidden layers to handle non-linearities. MSE serves as the loss function to minimize prediction inaccuracies, while the Adam optimizer is chosen for efficient training and faster convergence.

Once trained, the ANN can rapidly infer the MPP under various conditions, providing a robust and adaptive MPPT solution. The ANN can handle the non-linear and dynamic nature of PV systems more effectively than traditional algorithms, ensuring optimal performance even under challenging conditions such as partial shading and fluctuating irradiance [33].

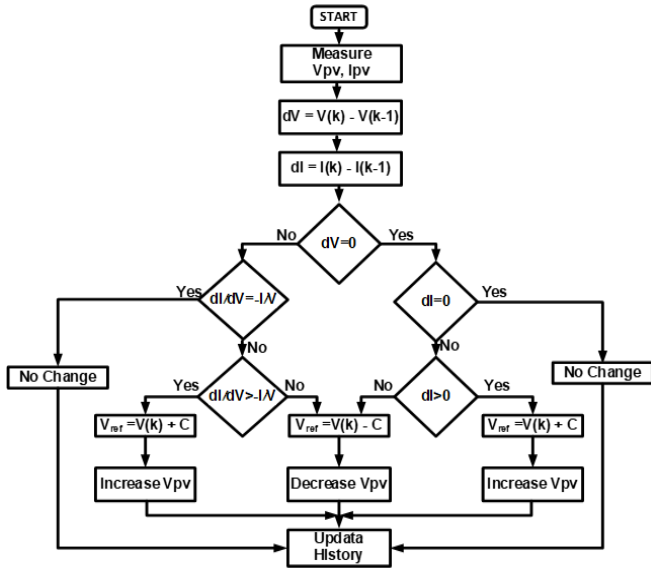


Figure 10. INC flow diagram [30]

## 5.1 INC

INC is used as the MPPT algorithm. The INC method aims to identify the direction of change in the terminal voltage of PV modules by measuring and comparing their INC with their instantaneous conductance. It solves the perturb and observes method limitations in tracking peak power in rapidly changing atmospheric circumstances. The basic theory is illustrated in Figure 9, and the operating flow diagram of the INC is shown in Figure 10.

When the operating point of PV modules is precisely at the MPP, the slope of the power curve is zero ( $dP/dV=0$ ), which can be further expressed using the relationship  $dP/dV=0$ . This means that incremental conductance ( $dI/dV$ ) equals instantaneous conductance ( $-I/V$ ), as shown in Eq. (13), which indicates that the maximum power and voltage points have been achieved.

$$\frac{dp}{dV} = \frac{d(VI)}{dV} = I + V \frac{dI}{dV} = 0 = \frac{dI}{dV} = -\frac{I}{V} \quad (13)$$

The PV module's output power ( $P_{out}$ ) is proportional to the terminal voltage if it operates in the constant current region. This means that the output power rises linearly with the PV module's rising terminal voltage, producing a positive slope on the power curve ( $dP/dV>0$ ). This indicates that the PV module's increased terminal voltage is the reason why the INC ( $dI/dV$ ) is greater than the instantaneous conductance ( $-I/V$ ), as Eq. (14) illustrates. The PV module's operating voltage on the PV diagram will be located to the left of the MPP, meaning that it must be increased to follow the MPP [30].

$$\frac{dp}{dV} > 0 = \frac{dI}{dV} > -\frac{I}{V} \quad (14)$$

If the  $P_{out}$  decreases linearly with the falling terminal voltage of the PV module, resulting in a negative slope on the power curve ( $dP/dV<0$ ). It signifies that the INC ( $dI/dV$ ) is reduced than the instantaneous conductance ( $-I/V$ ), as shown in Eq. (15), indicating the decreased terminal voltage of the PV module. The operating voltage of the PV module will be positioned to the right of the MPP on the PV diagram, indicating that it should be reduced to track the MPP.

Essentially, ANNs improve MPPT by learning complex relationships relating PV parameters to the MPP, adapting to fast environmental changes, and providing a more accurate and robust tracking solution. Thus, this makes them a valuable constituent of advanced PV system management strategies.

### 5.3 Hybrid MPPT combining INC and ANN

The hybrid technique combines two controllers: the ANN and INC methods to sustain maximum power and enhance efficiency under changing environmental conditions. The neural network consists of an input layer with two nodes, a hidden layer containing ten nodes, and an output layer with one node. The core concept of the hybrid algorithm is to utilize

the ANN controller to predict voltage values during insolation fluctuations, provided the irradiation changes are minimal. If the change is significant, the step size in the INC method becomes too small to reach the MPP, leading to oscillations [34]. The figure below illustrates the contemporary hybrid model control for MPPT. This approach's inputs include the PV panel's current, voltage, and power variation. The maximum power is determined using the neural network learning algorithm by adjusting the neurons' weights and integrating the results with those from the INC algorithm.

In this control approach, the ANN output is combined with the INC algorithm output, and the average duty cycle produced is sent to the PWM generator to create the switching pulses as shown in Figure 11.

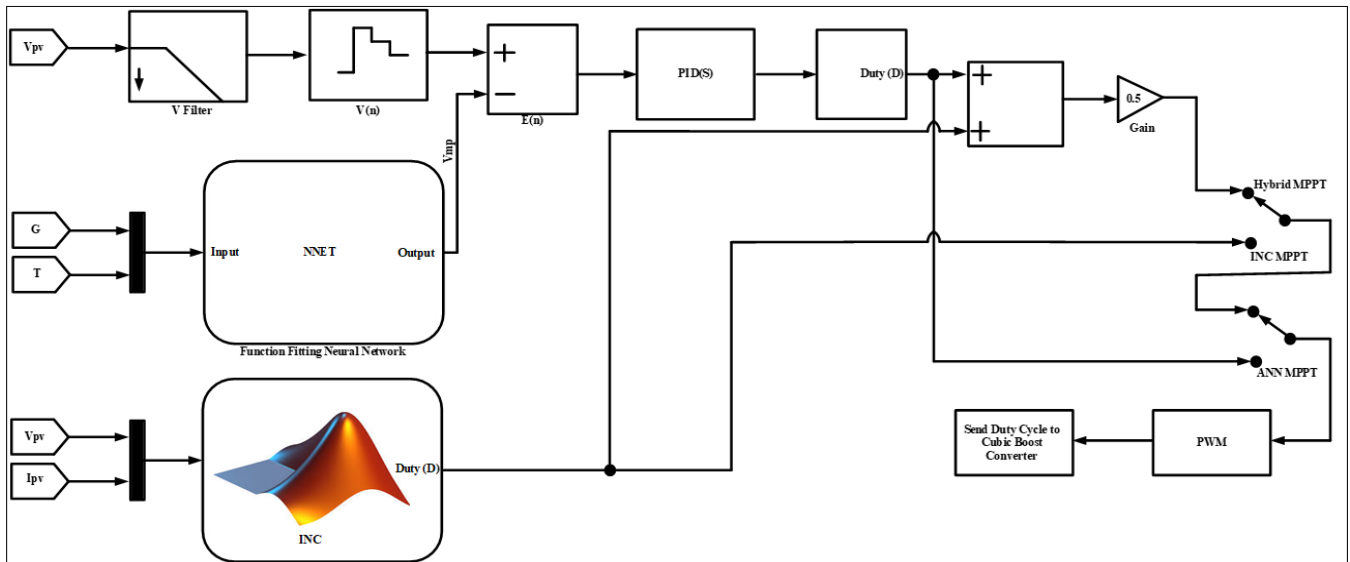


Figure 11. The flow diagram of the proposed hybrid-based MPPT for CBC

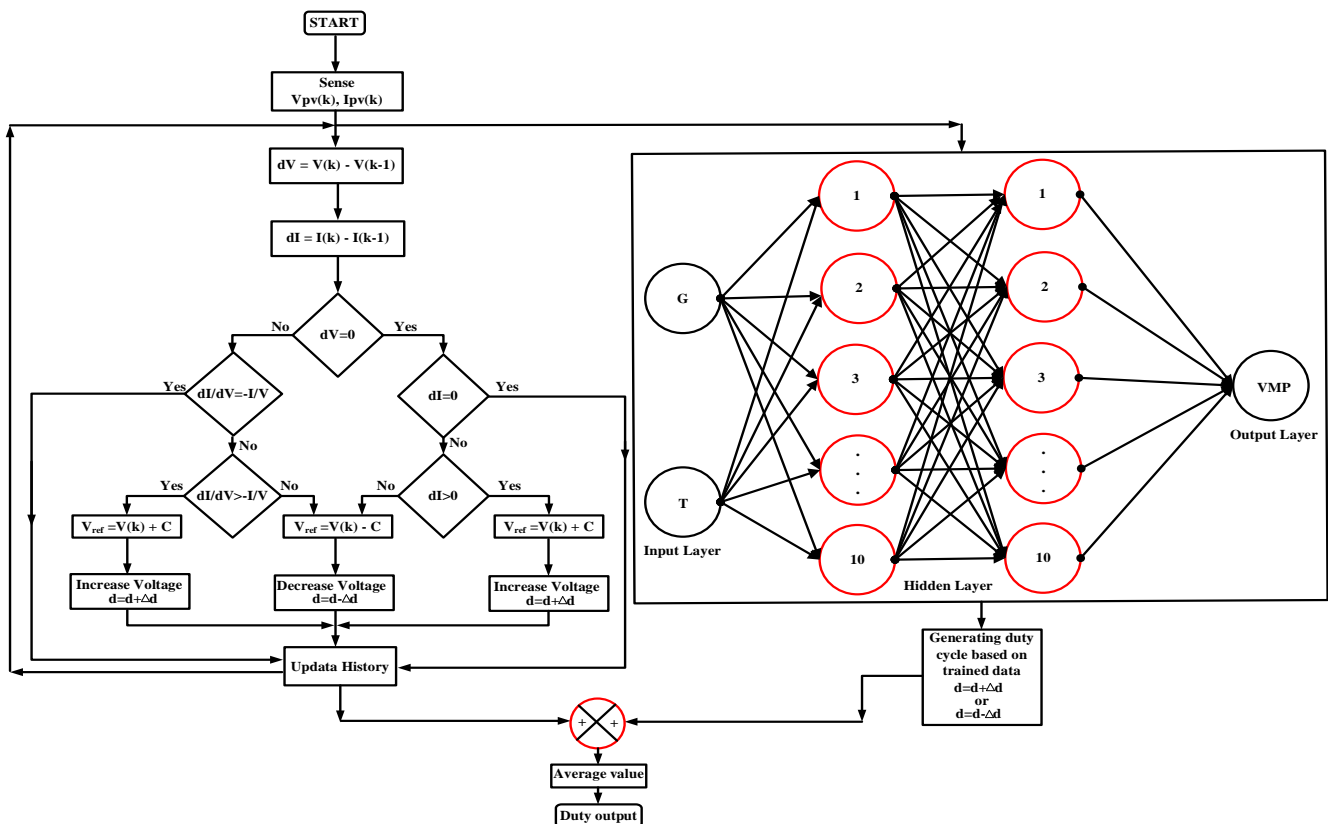


Figure 12. Flow chart for hybrid MPPT based on ANN and INC [35]

When the duty ratios from both methods are combined, the error in the duty cycle is minimized. This approach helps decrease oscillations around the maximum power point [35], as demonstrated in Figure 12.

The maximum power points for converter operation are determined by observing the power levels at various points using the INC method and the neural network approach.

Moreover, the maximum power is modified in response to environmental conditions. Unlike other complex hybrid methods for efficiently tracking the MPP, this strategy lowers system costs by decreasing the number of sensors needed. The hybrid techniques differ in their response speed, measurement assumptions, hardware implementation, number of sensors, and complexity.

$D_1$  represents the duty cycle produced by the ANN method, while  $D_2$  is the duty cycle generated by the INC. The combined result is given by  $D = (D_1 + D_2)/2$ .

The hybrid MPPT model [36], which combines the strengths of the INC algorithm and ANN, offers superior performance. Here is how the integration takes place:

**Initial Tracking with INC:** The INC algorithm is used for initial tracking due to its quick response to changes in operating conditions. It provides a reliable starting point for MPP tracking.

**ANN for Fine-Tuning:** The ANN then takes over for fine-tuning the tracking process against nonlinearities and disturbances to which it would be difficult for the INC algorithm alone to respond, like partial shading or fast irradiance changes.

**Dynamic Adjustment:** The current operating conditions dynamically switch between the INC algorithm and the ANN. In stable conditions, INC's algorithm can handle tracking; in fluctuating conditions, the ANN refines the prediction.

**Improved Efficiency and Robustness:** The hybrid model will integrate the INC algorithm's fast response with the ANN's adaptive learning ability to improve MPPT efficiency, dynamic response, and robustness against disturbances.

## 6. SIMULATION RESULT

The Hybrid INC-ANN Algorithm performs superiorly in tracking the MPP of solar panels compared to the use of standalone INC and ANN models, as shown in Table 2. The power tracking under varying environmental conditions, such as changes in irradiance and temperature, was consistently higher with the hybrid model, as shown in Figures 13 and 14.

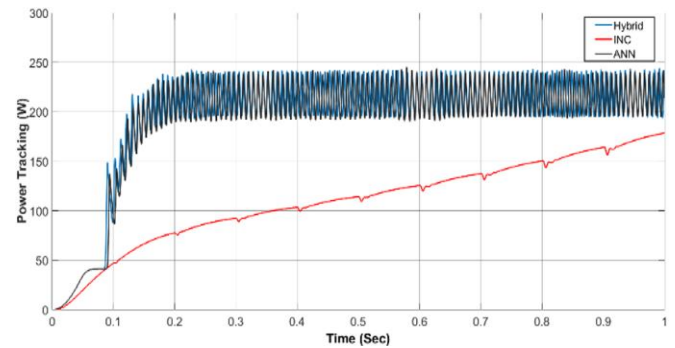


Figure 13. Power for hybrid, INC, and ANN when irradiation G=1000

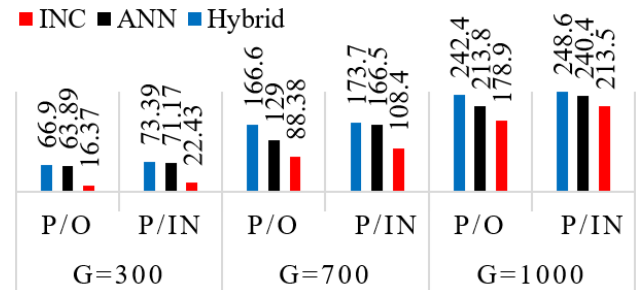


Figure 14. Maximum power and power tracking of MPPT algorithms with different irradiation

Table 2. Simulation results of MPPT algorithms with different irradiation

Irradiation Values (W/m <sup>2</sup> )	MPPT Methods	Maximum Power (W)	Power Tracking (W)	Voltage (V)	Current (I)	Efficiency
1000	INC	213.5	178.9	73.23	2.442	83.79
	ANN	240.4	213.8	80.06	2.67	88.94
	<b>Hybrid</b>	<b>248.6</b>	<b>242.4</b>	<b>85.24</b>	<b>2.843</b>	<b>97.48</b>
700	INC	108.4	88.38	51.48	1.717	81.52
	ANN	166.5	129	62.2	2.074	77.51
	<b>Hybrid</b>	<b>173.7</b>	<b>166.6</b>	<b>70.67</b>	<b>2.357</b>	<b>95.91</b>
300	INC	22.43	16.37	22.15	0.7389	72.99
	ANN	71.17	63.89	43.77	1.46	89.78
	<b>Hybrid</b>	<b>73.39</b>	<b>66.9</b>	<b>44.79</b>	<b>1.494</b>	<b>91.15</b>

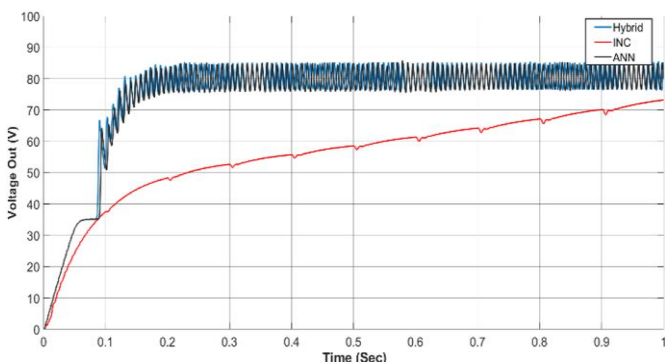


Figure 15. Voltage for hybrid, INC, and ANN when G=1000

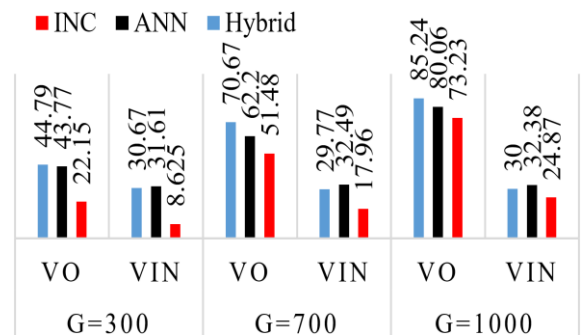
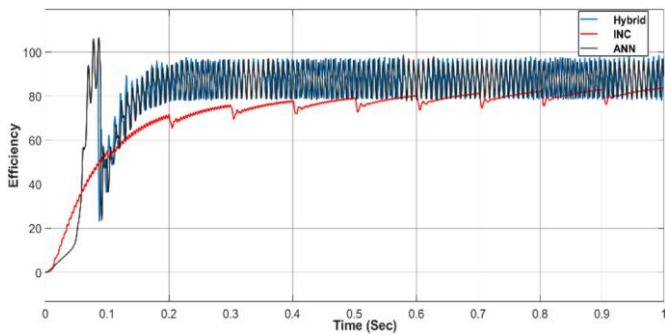
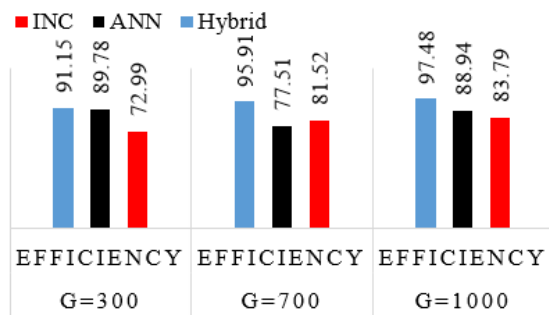


Figure 16. The voltage of MPPT algorithms with different irradiation



**Figure 17.** Efficiency for hybrid, INC, and ANN of G=1000



**Figure 18.** Efficiency of MPPT algorithms with different irradiation

**Table 3.** Comparison of different MPPT methods with related works

Ref.	Year	Method	Efficiency
[30]	2017	Hybrid (P&O+ANN)	89.4%
[35]	2022	Hybrid (P&O+ANN)	97.5%
[36]	2024	Hybrid (INC+ANN)	87.62%
This Work	2024	Hybrid (INC+ANN)	97.5%

The hybrid model's voltage regulation was more precise, maintaining the operating voltage closer to the MPP voltage, as shown in Figures 15 and 16. This precision in voltage tracking contributed to improved efficiency and power output.

The efficiency profile obtained from the hybrid model showed a smoother and more stable response to changes in environmental conditions. The hybrid model's ability to quickly adapt to variations in irradiance and temperature resulted in a more consistent efficiency, as shown in Figure 17. The ANN component of the hybrid model provided predictive adjustments. In contrast, the INC component fine-tuned the immediate response, minimizing oscillations around the MPP.

One such critical metric that can be used to evaluate MPP tracking algorithms is efficiency. As shown in Figure 18, the average efficiency using the hybrid ANN-INC model was 97.48%, much higher than that of the ANN model and the INC model, with efficiencies of 88.94% and 83.79%, respectively. This is attributed to the fact that the hybrid model manages to mix ANN's predictive qualities with the accuracy of INC in real-time, thus accomplishing effective and responsive MPP tracking. Table 3 shows the comparison of this proposed model with different MPPT-related works.

## 7. PRACTICAL AND IMPLEMENTATION

Implementing the high-gain cubic boost converter and hybrid MPPT in real-world solar PV systems requires careful

consideration. The performance of any converter depends on the availability of special components that can handle high power levels efficiently with good thermal management. Performances are affected under actual operating conditions, such as temperature variations, requiring reliable solutions.

The hybrid MPPT algorithm develops better power extraction by dynamic adaptation, while its complexity grows with the challenges in deployment and maintenance. Real-time processing demands may require advanced microcontrollers that will affect cost and power consumption. Integration into existing systems is the only way to take this into realistic implementation. Various possible limitations include reduced performance with partial shading and rapid weather changes. The system is scalable since it is modularly designed, though initial costs may be higher owing to the requirement for more specialized components. In the long run, energy efficiency can offset such costs. Hardware upgrades and compatibility with current systems will be needed for seamless integration.

The proposed system can be successfully implemented by realizing maximum benefits from its practical applications by making the possible limitations and drawbacks minimally effective.

## 8. CONCLUSION

The proposed paper presented a hybrid ANN-INC algorithm as an MPPT controller to track the MPP of solar panels more effectively. This proposed algorithm improved the inherent limitations of both artificial neural networks and incremental conductance techniques in conventional MPPT methods. The hybrid approach mitigated the inability of the ANN to reach the MPP under low solar irradiation and improved the tracking speed of the INC method. The simulation results for different levels of solar irradiation demonstrated the hybrid ANN-INC algorithm's superior operational characteristics in terms of fast convergence to the MPP, locating the MPP of the solar panel more precisely, and rapidly adapting to changes in solar irradiation. The hybrid ANN-INC model provided a mean efficiency of approximately 97.48% at radiation 1000 W/m<sup>2</sup> far higher than the standalone ANN and INC models at about 88.94% and 83.79%, respectively. When the radiation was 700 W/m<sup>2</sup>, the hybrid ANN-INC model provided an efficiency of approximately 95.91%, also higher than the standalone ANN and INC models at about 77.51% and 72.99%, respectively and radiation was 300 W/m<sup>2</sup>, the hybrid ANN-INC model provided an efficiency of approximately 91.15% also higher than the standalone ANN and INC models at about 89.78% and 72.99%, respectively. The results have demonstrated that the hybrid ANN-INC algorithm works by overcoming the shortcomings of traditional MPPT methods to deliver a resilient and efficient solution for maximizing power extraction from photovoltaic panels. This approach efficiently extracts maximum power even under fluctuating atmospheric conditions, providing higher power output than other techniques.

## 9. FUTURE WORK

Future studies are needed in several areas that hold the key to improving performance and making up for certain weaknesses within the system. Research into advanced

materials will help improve the thermal management of the system and its reliability. Stronger algorithms will allow the system to behave more adequately under dynamic environmental changes and lower response times when sudden weather changes occur. Integration of artificial intelligence in such systems further enhances predictability through adaptive control. Scalability studies are required for larger applications to establish that services can be provided at reasonable costs and must be compatible with available infrastructure. Finally, large-scale field trials yield valuable real-world data for further refinements and validation. In these manners, various current challenges can be met, and full potential achieved in practical applications.

## ACKNOWLEDGMENT

The authors would like to thank Al-Iraqia University for supporting this research.

## REFERENCES

- [1] Perera, F. (2018). Pollution from fossil-fuel combustion is the leading environmental threat to global pediatric health and equity: Solutions exist. *International Journal of Environmental Research and Public Health*, 15(1): 16. <https://doi.org/10.3390/ijerph15010016>
- [2] Mahler, R.L. (2023). Public views on the importance and expansion of renewable electricity production over the last 35 years in Idaho, USA. *International Journal of Energy Production and Management*, 8(3): 133-139. <https://doi.org/10.18280/ijepm.080301>
- [3] Khan, R.A., Liu, H.D., Lin, C.H., Lu, S.D., Yang, S.J., Sarwar, A. (2023). A novel high-voltage gain step-up DC-DC converter with maximum power point tracker for solar photovoltaic systems. *Processes*, 11(4): 1087. <https://doi.org/10.3390/pr11041087>
- [4] Aifan G. Alsulami, A., Alhussainy, A.A., Allehyani, A., Alturki, Y.A., Alghamdi, S.M., Alruwaili, M., Alharthi, Y.Z. (2024). A comparison of several maximum power point tracking algorithms for a photovoltaic power system. *Frontiers in Energy Research*, 12: 1413252. <https://doi.org/10.3389/fenrg.2024.1413252>
- [5] Saravanan, P., Cherukupalli, K., Jayaraman, R., Prakash, N.B. (2024). An analysis of the experimental configuration of a standalone PV system. *Tehnički Vjesnik*, 31(4): 1048-1054. <https://doi.org/10.17559/tv-20230628000768>
- [6] Kumar, V.H., Patel, R., Sahu, L.K., Kishor, Y. (2024). Solar photovoltaic-integrated energy storage system with a power electronic interface for operating a brushless DC drive-coupled agricultural load. *Energy Harvesting and Systems*, 11(1): 20230127. <https://doi.org/10.1515/ehs-2023-0127>
- [7] Choorakuzhiyil, A., Parate, K., Joshi, J. (2023). Comparative analysis of maximum power point tracking techniques for photovoltaic systems. In 2023 2nd International Conference for Innovation in Technology (INOCON), Bangalore, India, pp. 1-6. <https://doi.org/10.1109/INOCON57975.2023.10100994>
- [8] Arsa, I.S., Sutaya, I.W. (2023). Implementation of the MPPT short circuit method in determining the number of electrical load that can be supplied by solar panels. In IConVET 2022: Proceedings of the 5th International Conference on Vocational Education and Technology, Singaraja, Bali, Indonesia, p. 78. <https://doi.org/10.4108/eai.6-10-2022.2327351>
- [9] Baimel, D., Tapuchi, S., Levron, Y., Belikov, J. (2019). Improved fractional open circuit voltage MPPT methods for PV systems. *Electronics*, 8(3): 321. <https://doi.org/10.3390/electronics8030321>
- [10] Manohara, M., Bharadwaj, D.D., Reddy, K.A.K., Madhav, D.V., Ganesh, D.V., Thrinath, B.S. (2024). Analysis of perturb & observe MPPT algorithm in partial shading for DC-DC boost converters. In 2024 Second International Conference on Smart Technologies for Power and Renewable Energy (SPECon), Ernakulam, India, pp. 1-4. <https://doi.org/10.1109/specon61254.2024.10537508>
- [11] Chellakhi, A., El Beid, S., Abouelmahjoub, Y., Doubabi, H. (2024). An enhanced incremental conductance MPPT approach for PV power optimization: A simulation and experimental study. *Arabian Journal for Science and Engineering*, 49: 16045-16064. <https://doi.org/10.1007/s13369-024-08804-1>
- [12] Awan, M.M.A., Khan, A.U., Siddiqui, M.U., Karim, H., Bux, M. (2023). Optimized hill climbing algorithm for an islanded solar photovoltaic system. *Mehran University Research Journal of Engineering & Technology*, 42(2): 124-132. <https://doi.org/10.3316/informit.002522730337299>
- [13] Attalla, M.E., El-Sehiemy, R.A., El-Arwash, H.M. (2024). A fuzzy logic based maximum power point tracking of PV systems supplying remote sensing devices of two units cube satellite applications. *ERJ. Engineering Research Journal*, 47(3): 337-353. <https://doi.org/10.21608/erjm.2024.263628.1315>
- [14] Eltamaly, A.M., Al-Saud, M.S., Abokhalil, A.G. (2020). A novel scanning bat algorithm strategy for maximum power point tracker of partially shaded photovoltaic energy systems. *Ain Shams Engineering Journal*, 11(4): 1093-1103. <https://doi.org/10.1016/j.asej.2020.02.015>
- [15] Wirateruna, E.S., Millenia, A.F.A. (2022). Design of MPPT PV using particle swarm optimization algorithm under partial shading condition. *International Journal of Artificial Intelligence & Robotics*, 4(1): 24-30. <https://doi.org/10.25139/ijair.v4i1.4327>
- [16] de Oliveira, F.M., Brandt, M.H.M., Salvadori, F., Izquierdo, J.E.E., Cavallari, M.R., Ando Junior, O.H. (2024). Development of an MPPT-based genetic algorithm for photovoltaic systems versus classical MPPT techniques in scenarios with partial shading. *Inventions*, 9(3): 64. <https://doi.org/10.3390/inventions9030064>
- [17] Nezam, A.M., Mahmood, M.K., Karim, S.M., Addawe, A. (2024). Evaluation of incremental conductance MPPT algorithm under varying conditions. In 2024 21st International Multi-Conference on Systems, Signals & Devices (SSD), Erbil, Iraq, pp. 98-103. <https://doi.org/10.1109/SSD61670.2024.10548315>
- [18] Saadaoui, F., Mammari, K., Hazzab, A. (2019). Modeling of photovoltaic system with maximum power point tracking control by neural networks. *International Journal of Power Electronics and Drive Systems*, 10(3): 1575. <https://doi.org/10.11591/ijpeds.v10.i3.pp1575-1591>
- [19] Khan, F., Zaid, M., Tariq, A., Khan, M.M.A. (2023). A

- new non-isolated high-gain DC-DC converter for the PV application. *e-Prime-Advances in Electrical Engineering, Electronics and Energy*, 5: 100198. <https://doi.org/10.1016/j.prime.2023.100198>
- [20] Srinivas, B., Nagendrappa, H., Venkatesaperumal, B. (2024). A novel cubic boost converter with continuous source current for PV applications. *IEEE Transactions on Circuits and Systems II, Express Briefs*. <https://doi.org/10.1109/TCSII.2024.3434985>
- [21] Hachicha, A.A., Abo-Zahhad, E.M. (2023). Dust effect on solar energy systems and mitigation methods. *International Journal of Energy Production and Management*, 8(2): 97-105. <https://doi.org/10.18280/ijepm.080206>
- [22] Malik, P., Chandel, S.S. (2021). A new integrated single-diode solar cell model for photovoltaic power prediction with experimental validation under real outdoor conditions. *International Journal of Energy Research*, 45(1): 759-771. <https://doi.org/10.1002/er.5881>
- [23] Patil, S.R., Burade, P.G., Kadam, D.P. (2023). Five parameters extraction of single diode PV model by metaheuristic optimization method by identified built-up data. *Bulletin of Electrical Engineering and Informatics*, 12(3): 1371-1387. <https://doi.org/10.11591/eei.v12i3.4876>
- [24] Araújo, N.M.F.T.S., Sousa, F.J.P., Costa, F.B. (2020). Equivalent models for photovoltaic cell—A review. *Revista de Engenharia Térmica*, 19(2): 77-98. <https://doi.org/10.5380/reterm.v19i2.78625>
- [25] Jasim, A.M., Albaker, B.M., Jabir, H.J. (2024). Modeling and simulation of simplified quadruple diode solar PV module under influence of environmental conditions and parasitic resistance. *TEM Journal*, 13(1): 757-770. <https://doi.org/10.18421/TEM131-79>
- [26] Chaibi, Y., Allouhi, A., Malvoni, M., Salhi, M., Saadani, R. (2019). Solar irradiance and temperature influence on the photovoltaic cell equivalent-circuit models. *Solar Energy*, 188: 1102-1110. <https://doi.org/10.1016/j.solener.2019.07.005>
- [27] Yao, Q., Zeng, Y., Jia, Q. (2024). A novel non-isolated cubic DC-DC converter with high voltage gain for renewable energy power generation system. *Energy Engineering*, 121(1): 221-241. <https://doi.org/10.32604/ee.2023.041028>
- [28] Kathe, M.L., Makokha, A.B., Zachary, S.O., Adaramola, M.S. (2023). A comprehensive review of maximum power point tracking (MPPT) techniques used in solar PV systems. *Energies*, 16(5): 2206. <https://doi.org/10.3390/en16052206>
- [29] Sarvi, M., Azadian, A. (2022). A comprehensive review and classified comparison of MPPT algorithms in PV systems. *Energy Systems*, 13(2): 281-320. <https://doi.org/10.1007/s12667-021-00427-x>
- [30] Lodhi, E., Lodhi, Z., Shafiqat, R.N., Chen, F. (2017, July). Performance analysis of ‘perturb and observe’ and ‘incremental conductance’ MPPT algorithms for PV system. *IOP Conference Series: Materials Science and Engineering*, 220(1): 012029. <https://doi.org/10.1088/1757-899X/220/1/012029>
- [31] Mahmood, A.M., Abdul Zahra, M.M., Hamed, W., Bashar, B.S., Abdulaal, A.H., Alawsi, T., Adhab, A.H. (2022). Electricity demand prediction by a transformer-based model. *Majlesi Journal of Electrical Engineering*, 16(4): 97-102. <https://doi.org/10.30486/mjee.2022.696520>
- [32] Ibrahim, A.W., Ding, M., Jin, X., Dai, X., Sarhan, M.A., Shafik, M.B., Zhou, H. (2019). Artificial neural network based maximum power point tracking for PV system. In 2019 Chinese Control Conference (CCC), Guangzhou, China, pp. 6559-6564. <https://doi.org/10.23919/chicc.2019.8865275>
- [33] Sarwar, S., Javed, M.Y., Jaffery, M.H., Arshad, J., Ur Rehman, A., Shafiq, M., Choi, J.G. (2022). A novel hybrid MPPT technique to maximize power harvesting from PV system under partial and complex partial shading. *Applied Sciences*, 12(2): 587. <https://doi.org/10.3390/app12020587>
- [34] Habibi, M.N., Windarko, N.A., Tjahjono, A. (2019). Hybrid maximum power point tracking using artificial neural network-incremental conduction with short circuit current of solar panel. In 2019 International Electronics Symposium (IES), Surabaya, Indonesia, pp. 63-69. <https://doi.org/10.1109/elecsym.2019.890153>
- [35] Veerabhadra, Nagaraja Rao, S. (2022). Assessment of high-gain quadratic boost converter with hybrid-based maximum power point tracking technique for solar photovoltaic systems. *Clean Energy*, 6(4): 632-645. <https://doi.org/10.1093/ce/zkac041>
- [36] Bellah, B.M., Tahar, B., Adel, B. (2024). Adaptive hybrid MPPT using artificial intelligence for an autonomous PV system. *International Journal of Smart Grid-ijSmartGrid*, 8(1): 27-34. <https://doi.org/10.20508/ijsmartgrid.v8i1.328.g331>

## NOMENCLATURE

$I_{ph}$	Light-generated current source in (A)
$I_d$	Diode current in (A)
$I_p$	Parallel resistance current in (A)
$V_O$	Output voltage in (V)
$V_{oc}$	Open-circuit voltage in (V)
$V_{MP}$	Voltage at maximum power point in (V)
$I_{MP}$	Current at maximum power point in (A)
$P_{MP}$	Power at maximum power point in (W)
$I_C$	Output current in (A)
$I_s$	Diode saturation current in (A)
$I_{rs}$	Diode reverse saturation current in (A)
$I_{sc}$	Short-circuit current in (A)
$A$	Diode ideality factor, which =1.0189
$V_T$	Thermal voltage = 26 mV at 300 K
$n_s$	Cells connected in series
$n_p$	Cells connected in parallel
$K_B$	Boltzmann constant, which = $(1.381 \times 10^{-23} \text{ J/K})$
$q$	Charge of electron, which = $(1.6 \times 10^{-19} \text{ C})$
$T_{ref}$	Reference temperature = 298K
$T$	Operating temperature
$R_{se}$	Series resistance of a PV, which = 0.237 $\Omega$
$R_{pa}$	Parallel resistance of a PV, which =240.6 $\Omega$
$G_{pa}$	Parallel admittance of a PV
$E_g$	Band gap of the silicon, which =1.1 eV
$G_{ir}$	Irradiation in ( $\text{W/m}^2$ )
$G_{STC}$	Irradiation at standard test condition (STC), which = 1000 $\text{W/m}^2$
$I_{scSTC}$	Short circuit current of cell at (STC) (in Ampere), which happen with (T=25 short Cell’s short-circuit current

$K_{sc}$  Short is the cell's short-circuit current Temperature coefficient (A/K), which = 0.086998 mA/°C

$K_{ov}$  Cell's open-circuit voltage temperature coefficient (V/K), which = -0.369 m V/°C